Available online at www.sciencedirect.com
ScienceDirect
Journal of Solid State Chemistry 179 (2006) 3831–3838
JOURNAL OF SOLID STATE CHEMISTRY
www.elsevier.com/locate/jssc

Comparative study of $LiMn_2O_4$ thin film cathode grown at high, medium and low temperatures by pulsed laser deposition

S.B. Tang[a], M.O. Lai[a], L. Lu[a,*], S. Tripathy[b]

[a]Department of Mechanical Engineering, National University of Singapore, Singapore 117576, Singapore
[b]Institute of Materials Research and Engineering, 3, Research Link, Singapore 117602, Singapore

Received 18 May 2006; received in revised form 17 August 2006; accepted 24 August 2006
Available online 30 August 2006

Abstract

$LiMn_2O_4$ thin films with different crystallizations were respectively grown at high, medium and low temperatures by pulsed laser deposition (PLD). Structures, morphologies and electrochemical properties of these three types of thin films were comparatively studied. Films grown at high temperature ($\geqslant$873 K) possessed flat and smooth surfaces and were highly crystallized with different textures and crystal sizes depending on the deposition pressure of oxygen. However, films deposited at low temperature (473 K) had rough surfaces with amorphous characteristics. At medium temperature (673 K), the film was found to consist mainly of nano-crystals less than 100 nm with relatively loose and rough surfaces, but very dense as observed from the cross-section. The film deposited at 873 K and 100 mTorr of oxygen showed an initial discharge capacity of 54.3 $\mu Ah/cm^2\,\mu m$ and decayed at 0.28% per cycle, while the amorphous film had an initial discharge capacity of 20.2 $\mu Ah/cm^2\,\mu m$ and a loss rate of 0.29% per cycle. Compared with the highly crystallized and the amorphous films, nano-crystalline film exhibited higher potential, more capacity and much better cycling stability. As high as 61 $\mu Ah/cm^2\,\mu m$ of discharge capacity can be achieved with an average decaying rate of only 0.032% per cycle up to 500 cycles. The excellent performance of nano-crystalline film was correlated to its microstructures in the present study.

Keywords: $LiMn_2O_4$ thin films; Pulsed laser deposition; Nano-crystals; Capacity; Stability

1. Introduction

Spinel $LiMn_2O_4$ is an attractive cathode material for Li/Li^+ rechargeable batteries and has been extensively studied due to its high voltage, low cost and non-toxicity [1]. It may reversibly deintecalate one lithium per formula unit, with a theoretical capacity of 148 mAh/g [2], which corresponds to 63.6 $\mu Ah/cm^2\,\mu m$ in a thin film if a theoretical density of 4.3 g/cm^3 is assumed. However, compared with its counterpart $LiCoO_2$, the significant capacity decay of $LiMn_2O_4$ with extended cycling in powder electrode, especially at elevated temperatures, prevents its wide use in the commercial field [1]. Several factors including manganese dissolution, decomposition of electrolytes at high potentials and structural instability due to Jahn–Teller distortion have been postulated [3]. In order to improve the cycleability of $LiMn_2O_4$, transition-metal substitution of manganese in the spinel [4–6] and coating of various oxides have been investigated [7–9].

$LiMn_2O_4$ in the form of thin film has a potential application as a cathode in microbatteries, which have attracted much attention in recent years [10]. $LiMn_2O_4$ thin films have been prepared by various deposition techniques such as electron-beam evaporation [11], electrostatic spray deposition (ESD) [12], radio frequency (rf) sputtering [13,14] and pulsed laser deposition (PLD) [15–17]. Depending on the process conditions, thin film $LiMn_2O_4$ has shown better cycling stability than its powder [18,19]. Most of these studies have been focused on the electrochemical properties of highly crystallized $LiMn_2O_4$ by high-temperature post-annealing after deposition or direct high-temperature growth using PLD since it is generally believed that highly crystallized spinel structure of $LiMn_2O_4$ can provide three-dimensional networks for Li-ion transport. However, low-temperature processes have undoubtedly

*Corresponding author. Fax: +65 6779 1459.
E-mail addresses: mpeluli@nus.edu.sg, luli@nus.edu.sg (L. Lu).

0022-4596/$ - see front matter © 2006 Published by Elsevier Inc.
doi:10.1016/j.jssc.2006.08.025

more benefits in applications. Julien et al. [20] investigated the growth of $LiMn_2O_4$ thin films on silicon substrates at low temperatures ($\leqslant$573 K) by PLD and observed that a crystallized $LiMn_2O_4$ thin film was formed at 573 K using a lithium-rich target with 15% Li_2O excess. However, their films showed low discharge potentials (mainly below 4 V) and low capacity.

In the present paper, a comparative study on $LiMn_2O_4$ thin films deposited by PLD at high, medium and low temperature is reported. These films have been characterized by XRD, SEM, Raman and electrochemical measurement (charge/discharge, cyclic voltammetry (CV) and AC impedance).

2. Experimental

$LiMn_2O_4$ thin films were grown on polished stainless steel and Si substrates at different temperatures by PLD. A KrF laser beam (248 nm) with a pulse power of 160 mJ and frequency of 10 Hz was focused to a $LiMn_2O_4$ target supplied by SCI Engineered Materials Inc. (USA). The distance between target and substrate was 4 cm and the base pressure of the vacuum chamber was 2×10^{-5} Torr. The substrates were heated to the set temperature. Oxygen gas was then introduced and adjusted to the desired pressure. The films were grown while the target was rotating. The films were deposited in pairs, one on Si substrate for the cross-sectional SEM measurement, whereas the other on stainless steel substrate for electrochemical test and other characterizations. The thickness of the tested films was around 360 nm with an approximate deposition rate of 8 nm/min at 673 K and 200 mTorr of oxygen, 9 nm/min at 873 K and 100 mTorr of oxygen and 13 nm/min at 473 K and 200 mTorr of oxygen, respectively. The deposition rate normally decreases with the increase in pressure due to the contraction of plume in PLD. The relatively high deposition rate at 473 K and 200 mTorr of oxygen may be partially ascribed to the loose film.

A Shimadzu XRD-6000 diffractometer with a Cu$K\alpha$ source was used for characterization of crystallinity. The surface morphology of the films was observed using a Hitachi 4100 field-emission scanning electron microscope (FESEM). Thickness of the film was measured by cross-sectional SEM of films grown on Si substrates with about 0.2 μm top layer of SiO_2. Raman spectroscopy measurements were carried out using a Jobin-Yvon T64000 micro-Raman system equipped with a charge-coupled device (CCD) detector. Samples were excited by the polarized 514.5 nm line of Ar^+ laser at a power level of 5 mW. The laser spot size at the surface of the sample was about 1 μm while the spectrum resolution was about 0.5 cm^{-1}.

A half cell using a $LiMn_2O_4$ film of 10 mm diameter as cathode and Li metal foil as anode was assembled into a home-made Swagelok cell in an Ar-filled glove box with both H_2O and O_2 levels less than 0.1 ppm. The electrolyte was 1 M $LiPF_6$ in 1:1 ethylene carbonate (EC) and diethyl carbonate (DEC) solution. Electrochemical measurements were carried out using a Solartron 1287 electrochemical interface and 1260 frequency response analyzer. The charge and discharge tests were conducted between 3.0 and 4.5 V under constant current densities. CV was scanned between 3.5 and 4.5 V at a sweep rate of 0.2 mV/s. Electrochemical impedance spectrum (EIS) was conducted in a frequency range from 300 kHz to 0.005 Hz using an AC signal with 10 mV amplitude. The long-term cycling test of charge–discharge was also performed on a Marccor MC-4 battery test system with four channels.

3. Results and discussion

Fig. 1 shows the X-ray diffraction patterns of $LiMn_2O_4$ thin films deposited on stainless steel substrates at high, medium and low temperatures. Two different oxygen pressures of 100 and 200 mTorr were used at high temperatures. At 898 K and 200 mTorr of oxygen (Fig. 1a), the film shows strong (1 1 1) orientation accompanied with weak (311) and (511) diffractions. The peak (400) at 43.91° overlapped with that of the substrate. A very weak peak at 55.96° may be attributed to Mn_3O_4. The film grown at 873 K and 100 mTorr of oxygen showed similar XRD patterns as the regular spinel $LiMn_2O_4$ (Fig. 1b). Although both films grown at high temperatures have similar characteristics of polycrystalline spinel, the film grown at 898 K shows (1 1 1) preferred orientation, in view of the relatively high intensity of (222) peak compared with (311) peak. The film deposited at 673 K and 200 mTorr of oxygen has a relatively broad (1 1 1) and weak (311) and (440) peaks (Fig. 1c), while the film grown at 473 K exhibits mainly amorphous structure with just one

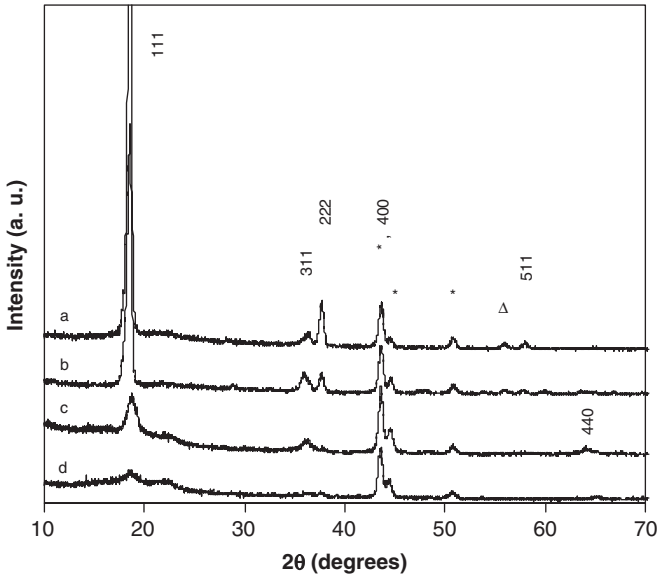

Fig. 1. XRD patterns of the as-deposited $LiMn_2O_4$ thin films on stainless steel substrates at different temperatures and oxygen pressures: (a) 898 K and 200 mTorr of oxygen; (b) 873 K and 100 mTorr of oxygen; (c) 673 K and 200 mTorr of oxygen and (d) 473 K and 200 mTorr of oxygen (* substrate, Δ Mn_3O_4).

weak and broad peak at around 18.7° (Fig. 1d). It is interesting that the former film grown at 673 K and 200 mTorr of oxygen has not shown any preferred orientation as that developed at high temperature (898 K and 200 mTorr of oxygen). The micro-Raman spectra of the as-deposited films on stainless steel substrates are shown in Fig. 2. The Raman spectra mainly consist of strong bands between 550 and 700 cm^{-1} and several weak bands in the range of 300–500 cm^{-1}. The Raman spectra of $LiMn_2O_4$ are complicated and the assignments are not unambiguous since they seem sensitive to the laser excitation and sometimes there appeared more number of vibrations than that predicated by group theory for the perfectly spinel compound [21,22]. For the films grown at high temperatures, there are two strong bands centered at around 629 and 659 cm^{-1} with a strong shoulder at 585 cm^{-1} in the high wavenumber region while three weak and broad bands located at around 480, 375 and 320 cm^{-1} are observable (Fig. 2a and b). The 631 cm^{-1} band becomes relatively stronger for the film deposited at 893 K and 200 mTorr of oxygen. The films grown at medium and low temperatures, however, show very different micro-Raman spectra in the high wavenumber region. The bands at 625 and 585 cm^{-1} become the shoulders of the main band at 654 cm^{-1} in the film grown at 473 K (Fig. 2d), while the shoulder at 625 cm^{-1} becomes obscure in the film grown at 673 K and the high wavenumber peak is thus narrow

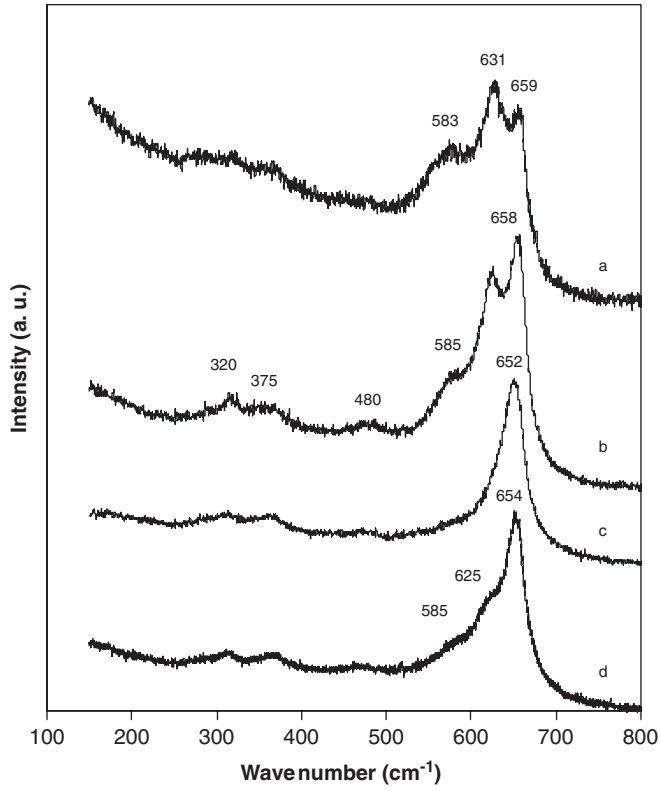

Fig. 2. Raman spectra of the as-deposited films on stainless steel substrates: (a) 898 K and 200 mTorr of oxygen; (b) 873 K and 100 mTorr of oxygen; (c) 673 K and 200 mTorr of oxygen and (d) 473 K and 200 mTorr of oxygen.

(Fig. 2c). The strong band located at around 654 cm^{-1} may be assigned to A_{1g} mode, corresponding to the symmetric Mn–O stretching vibration of MnO_6 groups, whereas the peaks located at 585, 480 and 375 cm^{-1} may be derived from three modes of T_{2g} phonons [22]. The assignment of band located at 629 cm^{-1} for high temperature processed films is not very clear and may be tentatively attributed to asymmetrical bonds of MnO_6 groups related to different Li coordinates. Chiu et al. [23] found that the band of A_{1g} mode at 630 cm^{-1} in their as-deposited film by RF sputtering shifted to 657 cm^{-1} after rapid thermal annealing (RTA) at 973 K. This shift is suggested to be related to a phase transition from the original spinel structure. This implies that the Raman spectra of $LiMn_2O_4$ depend on the processes of growth. The Raman spectra revealed different microstructures of $LiMn_2O_4$ films grown by PLD at high, and medium and low temperatures.

Fig. 3 shows the scanning electron micrographs of the as-deposited films on stainless steel substrates and cross-sectional SEM on Si substrates. The surfaces of the films grown at high temperatures are smooth and dense (Fig. 3a and b). The crystals in the film deposited at 898 K and 200 mTorr of oxygen are quite big of about 350 nm (Fig. 3a), while those grown at 873 K and 100 mTorr of oxygen are more uniform and small with an average size of about 250 nm (Fig. 3b). The high pressure of oxygen seems to promote crystallization and growth of crystals. Based on this observation, 200 mTorr of oxygen was used in the medium-and low-temperature depositions. The film grown at 673 K was mainly composed of fine nano-crystals less than 100 nm (Fig. 3c). The surface of this film was not as smooth and dense as those prepared at high temperatures, but it was much better than the low-temperature grown film (473 K), which mainly consists of large bean-pod shape grains and amorphous $LiMn_2O_4$ (Fig. 3d). These large bean-pod grains are not really crystals and may be some transition states between amorphous states and crystals. XRD thus detected just one weak and broad peak in this film (Fig. 1d). Cross-sectional SEM shows very dense nano-crystalline film and also a good contact with the substrate (Fig. 3f), compared with the highly crystallized film (Fig. 3e). This may be ascribed to the small grains in the nano-crystalline film.

Fig. 4 shows the cyclic voltammograms (CV) of the four $LiMn_2O_4$ thin films grown at different temperatures and oxygen pressures, and at a sweep rate of 0.2 mV/s. The CV curves are the fourth scan of the freshly assembled cells for the comparative purpose. Two couples of well-defined redox peaks at around 4.0 and 4.15 V were observed for the films grown at high (898 and 873 K) and medium temperature (683 K), corresponding to the two-step reversible de-intercalation and intercalation of lithium in $LiMn_2O_4$ [16]. However, the film grown at low temperature (473 K) showed no obvious redox peaks, a characteristic of amorphous $LiMn_2O_4$. The two films grown at high temperature with different pressures of oxygen displayed some differences, whereas the oxidation and reduction

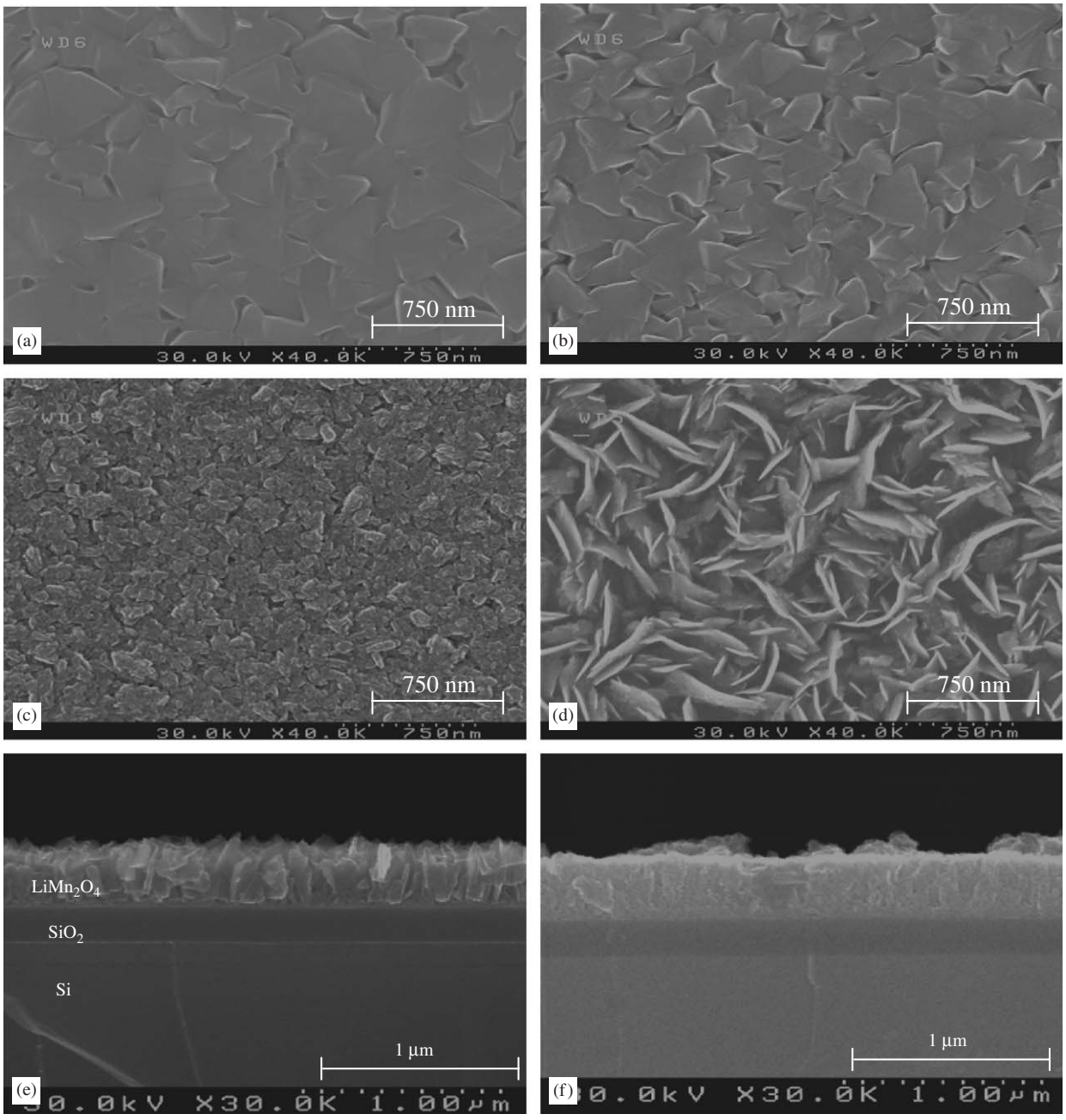

Fig. 3. SEM images of the as-deposited $LiMn_2O_4$ thin films on stainless steel substrates: (a) 898 K and 200 mTorr of oxygen; (b) 873 K and 100 mTorr of oxygen; (c) 673 K and 200 mTorr of oxygen; (d) 473 K and 200 mTorr of oxygen and cross-sectional images on Si substrates: (e) 898 K and 200 mTorr of oxygen; and (f) 673 K and 200 mTorr of oxygen.

peaks for the film grown at 873 K and 100 mTorr of oxygen are more symmetric with a little narrower peak separations than those for the film deposited at 898 K and 200 mTorr of oxygen. The former film has better reversibility while the latter film shows higher polarization and worse reversibility. Compared with the films processed at high temperatures, the nano-crystalline film grown at medium temperature (673 K and 200 mTorr of oxygen) exhibits another pair of high potential shoulder peaks at around 4.31 and 4.25 V, besides the two pairs of main oxidation/reduction peaks as marked on the curve (4.04 vs. 3.93 V and 4.18 vs. 4.10 V). This pair of peaks was observed for the first time in $LiMn_2O_4$ thin films, based on known literatures. Chiu et al. [14] have recently reported the nano-crystalline $Li_xMn_{2-y}O_4$ thin film prepared by biased RF sputtering deposition and post-annealing at 873 K. However, no obvious third pair of peaks at high potential in their CV curve up to 4.5 V could be found. The present nano-crystalline film may de-insert and insert more lithium above 4.2 V, resulting in a minor oxidation/reduction process or phase change that needs to be further clarified. Additionally, the main oxidation peaks are slightly shifted toward lower potentials and peak separation becomes further narrower (83 mV for the first pair of peak and

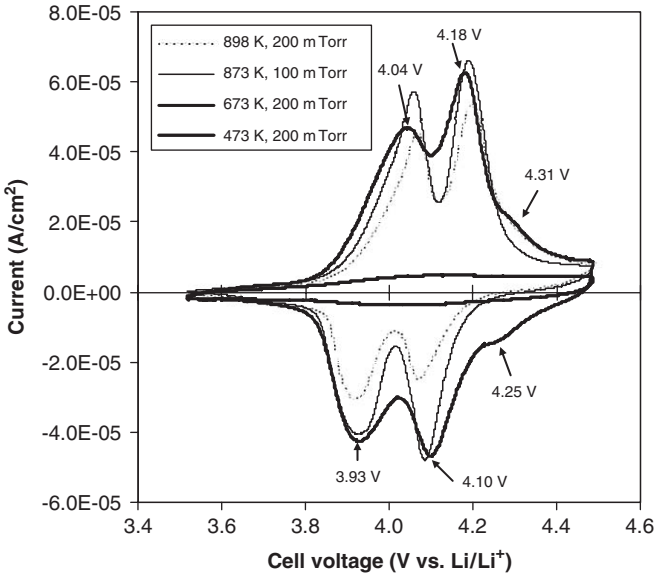

Fig. 4. Cyclic voltammograms of $LiMn_2O_4$ thin film electrodes deposited at different temperatures and constant scan rate of 0.2 mV/s.

113 mV for the second pair). The oxidation/reduction peaks are broad and quite symmetric. Higher capacity is thus expected to be achieved in the nano-crystalline $LiMn_2O_4$ film.

The AC impedance spectra of the three films at several potentials are shown in Fig. 5. Each Nyquist plot possesses a high-frequency depressed semicircle, a medium-frequency semicircle and a Warburg region followed by a steep sloping line at the lowest frequencies. As shown in Fig. 5a, the first small semicircle at high frequency is potential independent and the diameter of the second semicircle in the medium-frequency obviously changes with the potentials. The former may be ascribed to surface film formed on the surface of the electrode by electrolyte solution that also existed in other two samples (Fig. 5b and c). The latter is attributed to charge-transfer resistance related to slow Li^+-ion interfacial transfer. The semicircles in the high- and medium-frequency regions can be fitted using an equivalent circuit that is composed of parallel capacitance and resistance from the surface film and a double-layer capacitance (C_{dl}) and a charge-transfer resistance (R_{ct}). The charge-transfer resistance for the film deposited at 898 K and 100 mTorr of oxygen increases from 580 to 720 Ω with an increase in potentials from 3.9 to 4.2 V (660 Ω at 4.1 V). There is also a slight increase for the amorphous film grown at 473 K (290 Ω at 4.1 V in Fig. 5c). It is noted, however, that the charge-transfer resistance slightly decreases with the increment of potentials for the nano-crystalline film (325 Ω at 4.1 V in Fig. 5b). The nano-crystalline and amorphous films thus exhibited lower charge-transfer resistance.

Fig. 6 shows the changes of discharge capacity with cycle number of four films cycled between 3.0 and 4.5 V at a constant current density of 20 μAh/cm^2. The initial discharge capacity for the film grown at 898 K and 200 mTorr of oxygen was about 35.5 μAh/cm^2 μm and decayed continuously at about 0.69% per cycle, whereas the initial discharge capacity for the film deposited at 873 K and 100 mTorr reached 54.3 μAh/cm^2 μm and decayed at 0.28% per cycle. The former film has some large crystals of more than 400 nm that may not be fully accessible by Li-ion. Additionally, the film may contain higher Mn_3O_4 impurities and shows (1 1 1) preferred orientation as revealed by XRD. All these factors may lead to lower capacity and faster loss. The discharge capacity for the film grown at 873 K and 100 mTorr of oxygen is close to the value of a similar film reported by Striebel et al. (56 μAh/cm^2 μm cycled between 3.8 and 4.25 V) [18]. The nano-crystalline film grown at 673 K and 200 mTorr of oxygen had an initial discharge capacity of 59.6 μAh/cm^2 μm and achieved a maximum of 61 μAh/cm^2 μm during the 10th cycle, and then decayed at a very slow rate of only 0.03% per cycle. This phenomenon has frequently been observed in other nano-crystalline films such as Mg_2Si [24] and SnO_2 [25], though the mechanism leading to a slight increase of discharge capacity in the initial cycles is not very clear. Some restructure or surface reaction may be involved in the initial charge/discharge, in view of lower crystallization and higher surface area of nano-crystalline film [24]. The amorphous film showed much lower capacity with the initial discharge capacity of 20.2 μAh/cm^2 μm and a loss rate of 0.29% per cycle. The amorphous film has no well-formed network for Li-ion transport. Li-ion is mainly transported through the interstitial sites and its capacity should therefore be low. The large difference in electrochemical performance among four films indicates the size, and the orientation of crystals in high-temperature processed films seem to play an important role while the extent of crystallization in the medium- and low-temperature processed films should be more important.

Fig. 7 compares the charge and discharge curves of four films. All curves are present in the 10th cycle between 3.0 and 4.5 V with a current density of 20 μAh/cm^2. The amorphous film grown at 473 K and 200 mTorr of oxygen had smooth charge and discharge curves without obvious plateaus (curve a), whereas the two films processed at high temperatures showed two flat plateaus at around 4.0 and 4.15 V (curves b and c). The nano-crystalline film prepared at 673 K exhibited not only two little smooth plateaus, but also a short plateau near 4.25 V. Compared with the well-crystallized films, nano-crystalline film possessed not only relatively lower charge potentials, but also higher discharge potentials. The discharge capacity in the voltage range of 4.2–4.5 V took 13% of the corresponding total discharge capacity between 3 and 4.5 V for the nano-crystalline film, while the value was less than 3% for the highly crystallized films. This indicates that nano-crystalline film showed relatively more capacity at high potential above 4.2 V. These charge–discharge curves are in line with the CV curves shown in Fig. 4. It is interesting that the nano-crystalline film also showed some discharge capacity

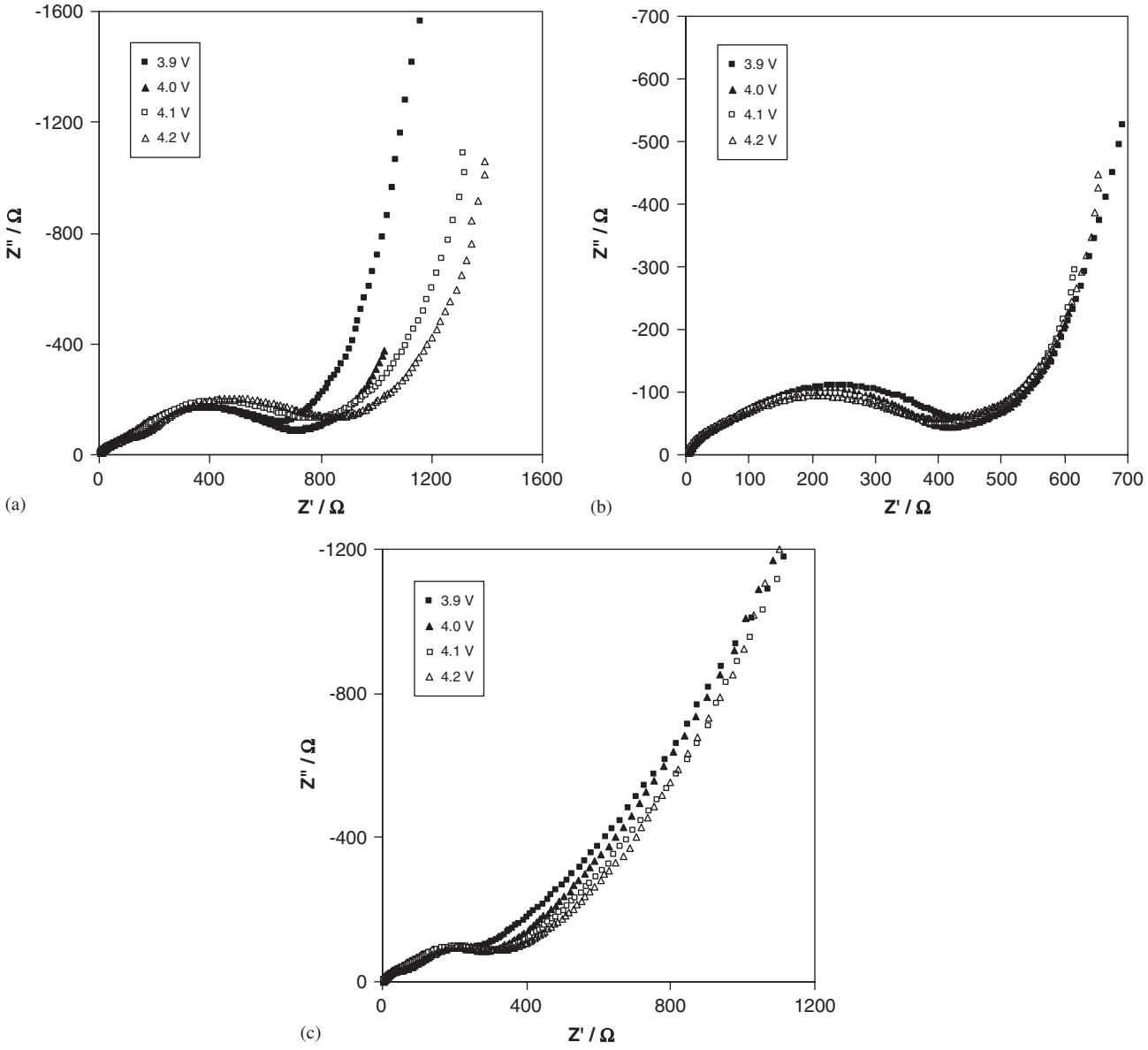

Fig. 5. AC impedance spectra of $LiMn_2O_4$ thin film cathodes deposited under 200 mTorr of oxygen and different temperatures: (a) 898 K, (b) 673 K and (c) 473 K.

between 3.3 and 3.0 V, which may be contributed from 3 V process corresponding to $x>1$ in $Li_xMn_2O_4$ [24]. $Li_xMn_2O_4$ cathode possesses both 4 V process cycled between 3.3 and 4.6 V ($0\leqslant x\leqslant 1$) and 3 V process in the voltage range of 2–3.3 V ($1\leqslant x\leqslant 2$). Most studies on $Li_xMn_2O_4$ have only been focusing on the 4 V process cycled between 3.3 and 4.35 V vs. Li/Li^+. Potential below and above these ranges are normally called overdischarge and overcharge, respectively [26]. In the present investigation, all films were charged and discharged between 3.0 and 4.5 V, involving partial overcharge and overdischarge in order to examine their cycleability. The more capacity in both high (>4.2 V) and low potential (<3.3 V) results in more total discharge capacity obtained over nano-crystalline film than that obtained from the highly crystallized films.

An extended charge–discharge cycling test up to 500 cycles was performed on the nano-crystalline film. As shown in Fig. 8, with a current density of 20 μAh/cm^2 in the first 100 cycles, the discharge capacity decayed at an average of 0.047% per cycle. The decay rate was 0.039% per cycle between cycles 101 and 300 with a current density of 60 μAh/cm^2, whereas the decay rate was only 0.019% per cycle from cycles 301–500 with a higher current density of 100 μAh/cm^2. This indicates that the nano-crystalline film became more stable with the extension of cycling since the rate of decay usually increases with the increase in charge/discharge current density. The average rate of decay was only about 0.032% per cycle up to 500 cycles regardless of the current density within 100 μAh/cm^2. Chiu et al. [14] recently found that the nano-crystalline thin-film cathode prepared by biased RF sputtering and

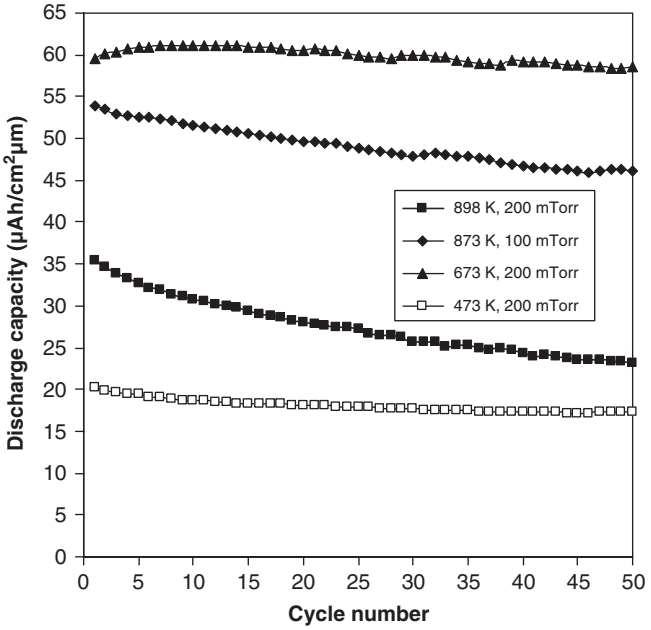

Fig. 6. The change in discharge capacity with the cycle numbers of $LiMn_2O_4$ thin film cathodes with a current density 20 μA/cm^2.

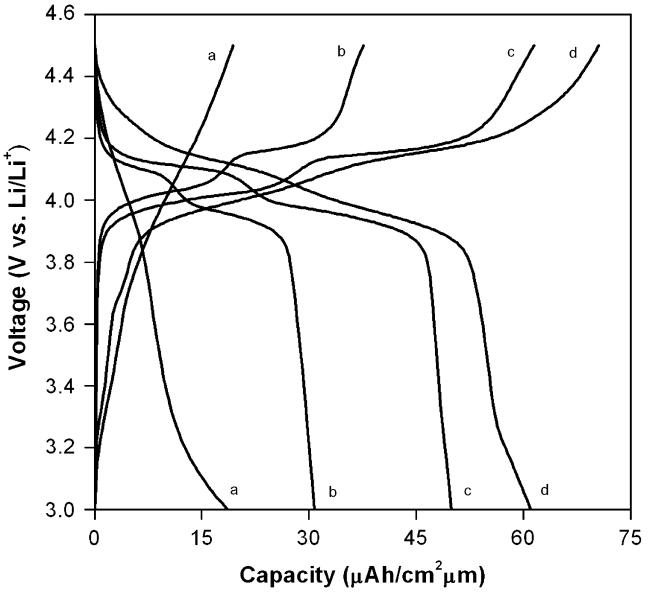

Fig. 7. Charge and discharge curves of $LiMn_2O_4$ thin film cathodes at 10th cycle with a current density 20 μA/cm^2: (a) 473 K and 200 mTorr of oxygen; (b) 898 K and 200 mTorr of oxygen; (c) 873 K and 100 mTorr of oxygen and (d) 673 K and 200 mTorr of oxygen.

post-annealing at 873 K showed better capacity retention although only a 30-cycle-duration was tested. Nano-crystals possess very small grains and high effective surface area that facilitate lithium diffusion into and out of the three-dimensional networks of crystals. Additionally, with the insertion of lithium ions, the original $LiMn_2O_4$ transforms to λ-MnO_2 that has a smaller lattice constant (8.03 Å) than that of spinel $LiMn_2O_4$ (8.24 Å) [27]. As shown in Fig. 1c, this nano-crystalline film possessed a little

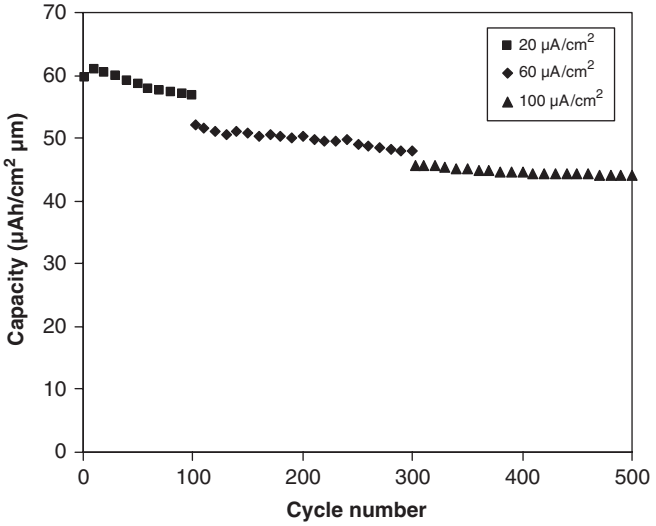

Fig. 8. Discharge capacity vs. cycle number of nano-crystalline $LiMn_2O_4$ film (grown at 673 K and 200 mTorr of oxygen) in extended cycling, with several current densities.

smaller lattice constant (higher 2θ value), closer to the lattice constant of λ-MnO_2, than that of the highly crystallized and coarse-grained $LiMn_2O_4$. The stress caused within the crystals with the Li-ion insertion/de-sertion is thus expected to be relatively smaller in this nano-crystalline film. All these factors may be beneficial to the capacity retention and extend the cycle life [28]. The excellent cycleability of the present nano-crystalline $LiMn_2O_4$ film prepared at medium temperature (673 K) is even better than that of highly crystallized $LiCoO_2$ film grown by a similar PLD method [29], bringing prospect in the application of microbatteries as a cathode. The detailed characterization of this nano-crystalline film and cycling stability at elevated temperature are still undergoing investigation and will be published elsewhere.

4. Conclusions

Highly crystallized, nano-crystalline and amorphous $LiMn_2O_4$ films deposited at different temperatures and oxygen pressures were comparatively studied and revealed very different capacities and retention of capacity. For the highly crystallized films, capacity and decaying rate of capacity seemed to depend on the size of crystal, purity and orientation. Too large crystals may not be fully accessible for Li-ion insertion/de-sertion, leading to a low capacity and a fast decay. Amorphous film has a low capacity due to the lack of three-dimensional networks for Li-ion transport.

The highest potential and capacity, and excellent cycleability have been achieved from nano-crystalline films. A small pair of anodic/cathodic peaks at around 4.25 V was observed for the first time besides the two main pairs of peaks at 4.0 and 4.15 V in CV of nano-crystalline $LiMn_2O_4$ films. The discharge capacity of nano-crystalline film reaches 61 μAh/cm^2 μm with a current density of

$20\,\mu Ah/cm^2$ and decays at an average rate of only 0.032% per cycle up to 500 cycles. The excellent performance of nano-crystalline $LiMn_2O_4$ film may be ascribed to a large effective surface area of the small nano-grains, relatively less stress within the grains during the lithium intercalation/de-intercalation and a good contact between active layer and substrates. Another advantage of this nano-crystalline film is the medium temperature growth process.

Acknowledgments

This work has been supported by the National University of Singapore under research grants R265-000-133-112 and R265-000-162-112.

References

[1] M. Broussely, P. Biensan, B. Simon, Electrochim. Acta 45 (1999) 3.
[2] M. Mohamedi, D. Takahashi, T. Itoh, I. Uchida, Electrochim. Acta 47 (2002) 3483.
[3] M.M. Thackery, Prog. Solid State Chem. 25 (1997) 1.
[4] M. Hosoya, H. Ikuta, M. Wakihara, Solid State Ionics 111 (1998) 153.
[5] A.R. Armstrong, P.G. Bruce, Nature 381 (1996) 499.
[6] H.-S. Moon, J.-W. Park, J. Power Sour. 119 (2003) 717.
[7] Z. Tang, Z. Zhang, W. Shen, Y. Lin, Solid State Ionics 148 (2002) 317.
[8] D. Shu, G. Kumar, K.B. Kima, K.S. Ryub, S.H. Chang, Solid State Ionics 160 (2003) 227.
[9] H.-S. Moon, S.-W. Lee, Y.-K. Lee, J.-W. Park, J. Power Sour. 119 (2003) 713.
[10] K.-L. Lee, J.-Y. Jung, S.-W. Lee, H.-S. Moon, J.-W. Park, J. Power Sour. 130 (2004) 241.
[11] M.M. Thackeray, J. Electrochem. Soc. 144 (1997) L100.
[12] J.-L. Shui, G.S. Jiang, S. Xie, C.H. Chen, Electrochim. Acta 49 (2004) 2209.
[13] H.-S. Moon, W. Lee, P.J. Reucroft, J.-W. Park, J. Power Sour. 119 (2003) 710.
[14] K.-F. Chiu, H.C. Lin, K.M. Lin, C.H. Tsai, J. Electrochem. Soc. 152 (1952) A2058.
[15] A. Rougier, K.A. Striebel, S.J. Wen, T.J. Richardson, R.P. Reade, E.J. Cairns, Appl. Surf. Sci. 134 (1998) 107.
[16] M. Morcrette, P. Barboux, J. Perriere, T. Brousse, A. Traverse, J.P. Boilot, Solid State Ionics 138 (2001) 213.
[17] I. Yamada, T. Abe, Y. Iriyama, Z. Ogumi, Electrochem. Commun. 5 (2003) 502.
[18] K.A. Striebel, C.Z. Deng, S.J. Wen, E.J. Cairns, J. Electrochem. Soc. 143 (1996) 1821.
[19] J.B. Bates, N.J. Dudney, B. Neudecker, A. Ueda, C.D. Evans, Solid State Ionics 135 (2000) 33.
[20] C. Julien, E. Haro-Poniatowski, M.A. Camacho-Lopez, L. Escobar-Alarcon, J. Jimenez-Jarquin, Mat. Sci. Engi. B 72 (2000) 36.
[21] A. Paolone, A. Sacchetti, T. Corridoni, P. Postorino, R. Cantelli, G. Rousse, C. Masquelier, Solid State Ionics 170 (2004) 135.
[22] B. Ammundsen, G.R. Burns, M.S. Islam, H. Kanoh, J. Roziere, J. Phys. Chem. B 103 (1999) 5175.
[23] K.-F. Chiu, H.H. Hsiao, G.S. Chen, H.L. Liu, J.L. Her, H.C. Lin, J. Electrochem. Soc. 151 (2004) A452.
[24] S.-W. Song, K.A. Striebel, R.P. Reade, G.A. Roberts, E.J. Cairns, J. Electrochem. Soc. 150 (2003) A121.
[25] R. Retoux, T. Brousse, D.M. Schleich, J. Electrochem. Soc. 146 (1999) 2472.
[26] A. Rougier, K.A. Striebel, S.J. Wen, E.J. Cairns, J. Electrochem. Soc. 145 (1998) 2975.
[27] E. Levi, M.D. Levi, G. Salitra, D. Aurbach, R. Oesten, U. Heider, L. Heider, Solid State Ionics 126 (1999) 109.
[28] F.K. Shokoohi, J.M. Tarascon, B.J. Wilkens, D. Guyomard, C.C. Chang, J. Electrochem. Soc. 139 (1992) 1835.
[29] S.B. Tang, L. Lu, M.O. Lai, Philos. Mag. 85 (2005) 2831.